*J. Fluid Mech.* (1992), *vol.* 236, *pp.* 95–110
*Printed in Great Britain*



# The concentration distribution near a continuous point source in steady homogeneous shear

By JAMES D. BOWEN† AND KEITH D. STOLZENBACH
Ralph M. Parsons Laboratory, Department of Civil Engineering, Massachusetts Institute of Technology, Cambridge, MA 02139, USA

(Received 3 April 1989 and in revised form 26 July 1991)

The concentration distribution resulting from a continuous point source in a fluid with a steady linear variation in velocity is distorted by the flow at distances greater than $(\kappa/E_b)^{\frac{1}{2}}$, where $\kappa$ is the molecular diffusion coefficient and $E_b$ is a characteristic shear rate. The distribution has two distinct shapes depending on the number of principal axes of fluid strain that are expansive and the relative magnitude of irrotational and rotational shears. For irrotational flows a single expansive principal axis of strain results in a tube-like distribution, while two expansive axes results in a disk-like distribution. Approximate analytical solutions, derived by neglecting diffusion along the expansive axes, agree well with concentrations calculated by numerically convolving the exact instantaneous source solution. The effect of fluid vorticity is generally to reorient the distribution away from the principal axes of strain and to reduce the asymmetry of the concentration distribution. Aside from reorientation, the concentration distribution varies little until the vorticity approaches a critical value defined by a kinematic condition for equilibrium orientation in the presence of rotation. For vorticity greater than the critical value, the concentration distribution becomes axisymmetric around the axis of rotation. Application of these results to numerical simulations of isotropic turbulence suggests that tubes are more common than disks and that vorticity exceeds the critical value in at least 25% of the fluid.

## 1. Introduction

In this article we consider the concentration distribution resulting from a continuous point source of soluble mass into an incompressible fluid with a steady velocity that is a homogeneous linear function of the distance from the point of input and which may be either irrotational or rotational. Of particular interest are the qualitative and quantitative features of the concentration distribution far enough from the source to be affected by the fluid motion but sufficiently close that the assumptions of steady homogeneous shear are valid for real flows. The analysis presented here will be applicable to mass transfer from a finite-sized particle as long as the Péclet number based on the particle diameter and the shear rate is small (Batchelor 1979).

In general we seek solutions to the advection–diffusion equation, given here in the steady-state form as

$$U_i \frac{\partial C}{\partial x_i} = \kappa \frac{\partial^2 C}{\partial x_i \partial x_i}, \tag{1.1}$$

where $C$ is the dissolved constituent concentration, $\boldsymbol{x}$ is the position vector from the

† Author to whom correspondence should be sent, at: ENSR Consulting and Engineering, 35 Nagog Park, Acton, MA 01720, USA.

point of mass input, and $\kappa$ is the molecular diffusion coefficient. The boundary conditions are

$$\left.\begin{aligned} C &\to 0 \quad \text{as} \quad r \to \infty, \\ 4\pi r^2 \kappa \frac{\mathrm{d}C}{\mathrm{d}r} &= F \quad \text{as} \quad r \to 0, \end{aligned}\right\} \tag{1.2}$$

where $F$ is the steady mass input rate and $r = (x_i x_i)^{\frac{1}{2}}$ is the distance from the point source. The general linear form for the relative fluid velocity $\boldsymbol{U}$ is

$$U_i = G_{ij} x_j = (E_{ij} + \Omega_{ij}) x_j, \tag{1.3}$$

where the velocity gradient tensor $\boldsymbol{G}$ is split into symmetric and antisymmetric parts, $\boldsymbol{E}$ and $\boldsymbol{\Omega}$ respectively, subject to the continuity constraint for an incompressible fluid $E_{ii} = G_{ii} = 0$. The elements of the velocity gradient tensor $\boldsymbol{G}$ are assumed to be constant in time and space.

Little previous work has been done on the concentration distributions for continuous point sources in flows with general linear velocity distributions. Analytical solutions are available for a continuous point source in a steady uniform stream (Carslaw & Jaeger 1959) and numerical solutions for continuous sources in two-dimensional shear flows have been presented (Csanady 1973; Okubo & Karweit 1969). Turfus (1986) examined concentration distributions near steady line sources in reversing shear flow and developed exact solutions as infinite series and/or integrals.

In contrast, the problem of diffusion of instantaneous sources in isotropic turbulence has a long theoretical and experimental history. The diffusion of heat spots in irrotational sheared flow was investigated by Townsend (1951*a*) whose equations for heat spot dispersal agreed well with experiments using hot-wire anemometry. The problem of diffusion of instantaneous sources in simple sheared flows was solved first by Novikov (1958) and again by Elrick (1962). Lumley (1972) investigated the effects of vorticity on the dispersal of point sources in two-dimensional shearing flow. The instantaneous source solution for a general linear flow was given by Batchelor (1979) and by Foister & Van de Ven (1980). The dispersion of contaminant clouds has been analysed for a variety of shear flows including the effects of boundaries and unsteadiness in the flow (Smith 1981, 1982).

In this article we discuss several new results relating to the concentration distribution surrounding a continuous source in a general linear shear flow with and without vorticity. Approximate analytical solutions for the irrotational case are derived and used to assess how the decrease in concentration along the principal axes of shear is influenced by the magnitudes of the principal shears. We show theoretically that the effect of fluid rotation on the concentration distribution depends on whether the vorticity is less than or greater than a critical value determined by the velocity gradient tensor. These results are evaluated quantitatively using a straightforward numerical convolution of the exact instantaneous source solution. The critical vorticity concept is used to infer a qualitative picture of concentration distributions surrounding point sources in isotropic turbulence.

## 2. General solution for steady point sources

The concentration for any location $\boldsymbol{x}$ surrounding the point of input for a continuous source can be given by convolution of the solution for an instantaneous source as

$$C(\boldsymbol{x}) = \frac{F}{(2\pi)^{\frac{3}{2}}} \int_0^\infty I^{-\frac{1}{2}} \exp\left(-\tfrac{1}{2} I^{-1}_{pq} x_p x_q\right) \mathrm{d}t, \tag{2.1}$$

where $\boldsymbol{I}$ is the second moment tensor for an instantaneous pulse defined as (Tennekes & Lumley 1972)

$$I_{pq}(t) = \iiint_{-\infty}^{\infty} x_p x_q C(\boldsymbol{x}, t)\, \mathrm{d}x_1 \mathrm{d}x_2 \mathrm{d}x_3. \tag{2.2}$$

A generalized Gaussian concentration distribution with second moments defined by $\boldsymbol{I}$ is a solution for the instantaneous point release provided that $\boldsymbol{I}$ satisfies the following ordinary differential equation (Batchelor 1979; Foister & Van den Ven 1980)

$$\frac{\mathrm{d}I_{pq}}{\mathrm{d}t} - I_{pj} G_{qj} - I_{qj} G_{pj} = 2\kappa\delta_{pq}, \tag{2.3}$$

where $\delta_{pq}$ is the Kronicker delta.

Concentration distributions around continuous sources for general velocity gradient tensors were calculated using a numerical integration of (2.1), obtained by summing the contributions of a finite number of instantaneous pulses. The time evolution of the second moment tensor $\boldsymbol{I}$, (2.3), for each instantaneous pulse was solved with an explicit finite-difference method. The time step of the finite-difference approximation was limited to be no more than 0.5% of minimum value of $1/G_{ij}$. Sensitivity analysis was conducted to determine the minimum number of pulses necessary for the numerical convolution and the evolution of the second moment tensor $\boldsymbol{I}$ was compared with the analytical solution for irrotational shear, (3.2) (Townsend 1951*a*). The numerically derived concentration distribution for motionless diffusion was compared with the analytical solution $C = F/4\pi\kappa r$ (Carslaw & Jaeger 1959).

## 3. Point sources in steady irrotational shear

In the special case where the rotational, antisymmetric component of the velocity gradient tensor is zero ($\boldsymbol{\Omega} = 0$), the velocity gradient tensor given as $\boldsymbol{G} = \boldsymbol{E}$ will be symmetric and can be simplified as

$$E_i = G_{pq}\, \xi_p^{(i)}\, \xi_q^{(i)}, \tag{3.1}$$

where $E_i$ is the extension rate along the symmetric tensor's $i$th principal axis, whose unit position vector is $\xi^{(i)}$. For irrotational shearing, with velocity gradients steady in time, the second moment tensor of an instantaneous pulse, $\boldsymbol{I}$, is (Townsend 1951*a*)

$$\left.\begin{aligned} I_i(t) = I_{ij}(t) = \frac{\kappa}{E_i}(\exp 2E_j t - 1) \quad & (i = j), \\ I_{ij}(t) = 0 \quad & (i \neq j). \end{aligned}\right\} \tag{3.2}$$

The transformation to the principal axis for $\boldsymbol{G}$, defined by $\xi^{(i)}$, also diagonalizes $\boldsymbol{I}(t)$, thus the principal axes of strain are also the principal axes for the instantaneous pulse. The dimensions of the pulse increase exponentially with time along expansive axes ($E_j > 0$) and approach a constant along compressive axes, that is $I_i = -\kappa/E_i$ for $t \gg 1/-E_j$ and $E_j < 0$. The concentration distribution for a continuous release can be found by integrating the instantaneous source solution as

$$C(\boldsymbol{x}) = \frac{F(E_1 E_2 E_3)^{\frac{1}{2}}}{(2\pi\kappa)^{\frac{3}{2}}} \int_0^{\infty} \frac{1}{[\Pi_{j-1}^{3}(\exp 2E_j t - 1)]} \exp\left[\frac{-E_i x_i x_i}{2\kappa(\exp 2E_i t - 1)}\right] \mathrm{d}t. \tag{3.3}$$

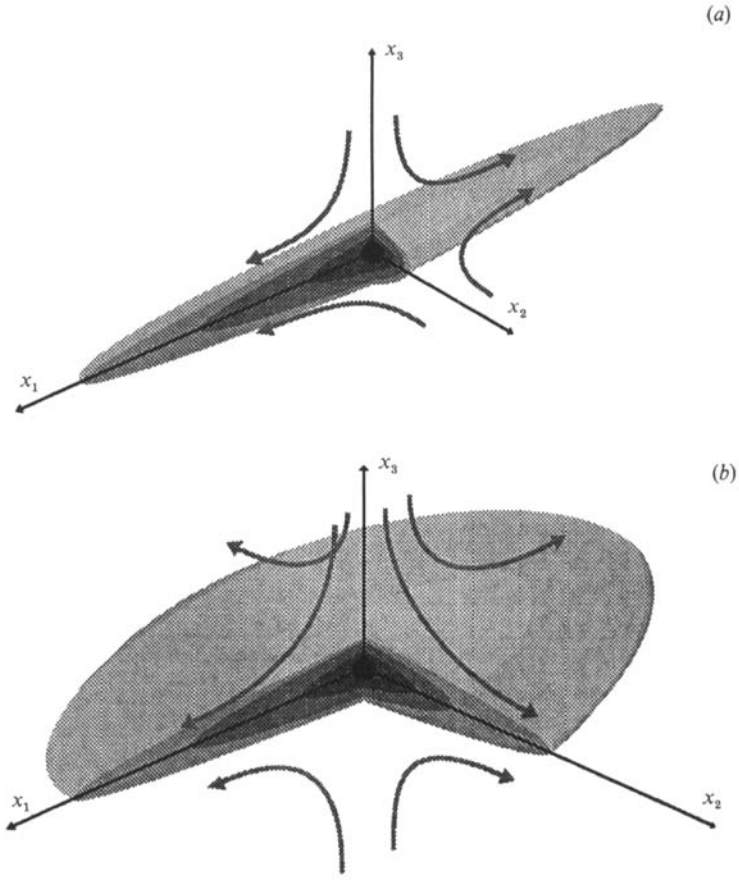


FIGURE 1. Qualitative features of concentration distributions for continuous point sources in steady homogeneous shear flows. The dark sphere at the origin has a radius of $(\kappa/E_b)^{\frac{1}{2}}$ that indicates the size of the diffusive region unaffected by the fluid motion. The lighter shading concentration contours distorted by shearing flow. The arrows indicate the fluid streamlines. (*a*) Tube: $E_1 > 0$, $E_2$ and $E_3 < 0$. (*b*) Disk: $E_1$ and $E_2 > 0$, $E_3 < 0$.

The form of the solution to (3.3) depends on the signs and magnitudes of the shear components. To simplify the specification of these components we adopt the following conventions, noting that $\sum_{i=1}^{3} E_i = 0$ from continuity, and $(E_i E_i)^{\frac{1}{2}} \neq 0$ for sheared flows. Because of the flow field's symmetry about the origin we choose, with no loss of generality, the principal axes so that $E_1 > E_2 > E_3$, which requires that $E_1 > 0$ and $E_3 < 0$. The shear tensor can then be completely specified with two parameters, which are

$$\left.\begin{aligned} E_b &= \tfrac{1}{2}\sum_{i=1}^{3}\left|E_i\right|, \\ s &= \frac{2E_2}{E_b} \quad (-1 < s < 1), \end{aligned}\right\} \tag{3.4}$$

where $E_b$ specifies the strength of the shearing while $s$ is a symmetry factor such that $s = 1$ is an expansive shear flow axisymmetric about $x_3$ and $s = -1$ is a compressive shear flow axisymmetric about $x_1$.

### 3.1. *Qualitative features of the continuous point source solution*

Two distinct concentration distributions result for continuous sources depending on the number of expansive axes. When the flow is compressive along two axes ($s < 0$), concentration gradients along these axes are steeper than along the single expansive axis, resulting in concentration contours distorted by the flow into tube-like structures (figure 1*a*). A structure similar to the tube results when the shear along $x_2$ is absent ($s = 0$) and is referred to as a diffusive tube since the transport in the $x_2$ direction is diffusive. When the flow is expansive along $x_1$ and $x_2$ ($s > 1$), the distribution becomes flattened along the compressive $x_3$ axes, and disk-like concentration contours are produced (figure 1*b*). For both tubes and disks the concentration distributions are oriented along the principal axes of strain. Near the source, where the relative fluid velocity is small, the concentration contours are spherical (figure 1). The shape and orientation of concentration distributions for instantaneous point sources show a similar behaviour (Townsend 1951*a*). This similarity is not surprising because in shearing flows elements of the second moment tensor grow exponentially in time, thus only a narrow range of times contribute to the convolution integral describing the concentration distribution for a continuous source (3.3).

## 4. Approximate analytical solutions in the sheared region of irrotational flow

The qualitative and quantitative features of the concentration distributions and the convolution integral from which they arise suggest that approximate analytical equations can be developed for the region where transport by the shear flow dominates diffusive transport. Within this sheared region we assume that the flux of material away from the source is due entirely to advection along the expansive axes and that the times contributing to the convolution integral, (2.1), will be greater than $1/-E_i$, where $E_i$ is the strain rate along compressive axes. Thus concentration distributions along compressive axes will be approximately Gaussian with a variance of $\kappa/-E_i$. Approximate analytical solutions for the concentration distributions can then be found by writing a flux equation using the assumed form of the concentration distribution.

Concentration distributions are normalized by defining the characteristic quantities

$$x_0 = \left(\frac{\kappa}{E_b}\right)^{\frac{1}{2}}, \quad C_0 = \frac{F E_b^{\frac{1}{2}}}{4\pi\kappa^{\frac{3}{2}}}, \tag{4.1}$$

where the length $x_0$ is the Batchelor scale where diffusive and advective dispersal are of the same magnitude (Batchelor 1959), and the concentration $C_0$ is the concentration that would result at $r = x_0$ in the complete absence of motion. The following sections give approximate analytical solutions for each of the shear patterns described earlier.

### 4.1. *Tube*

For a tube $E_1 = E_b$, $E_2, E_3 < 0$. The assumed concentration distribution is

$$C(\boldsymbol{x}) = C_c \exp\left[\frac{E_2 x_2^2}{2\kappa} + \frac{E_3 x_3^2}{2\kappa}\right], \tag{4.2}$$

where $C_c$ is the concentration along the expansive $x_1$ axis. The flux equation is given as

$$F = 2\int\int_{-\infty}^{\infty} u_1(x_1)\, C(\boldsymbol{x})\, \mathrm{d}x_2\, \mathrm{d}x_3 = 2E_1 x_1\, C_c(x_1) \int\int_{-\infty}^{\infty} \exp\left[\frac{E_2 x_2^2}{2\kappa} + \frac{E_3 x_3^2}{2\kappa}\right] \mathrm{d}x_2\, \mathrm{d}x_3. \quad (4.3)$$

Integration of the flux relation in the two compressive flow directions results in the following equation for the centreline concentration

$$C_c(x_1) = \tfrac{1}{2} C_0 \frac{-x_0\, s(s+2)}{|x_1|}. \quad (4.4)$$

Along the tube centreline, concentrations fall off as for the case without motion, i.e. independent of the rate of strain. Concentration levels are, however, dependent on the symmetry of the shearing in compressive directions, as represented by $s$. Axisymmetric tubes ($s = -1$) have centreline concentrations equal to one-half the value for a continuous source in motionless fluid. Comparison with the exact numerically derived solution for an axisymmetric tube shows that the concentration distribution given by (4.2) and (4.4) agrees well in the region where advective effects are dominant ($r > x_0$) (figure 2).

### 4.2. *Diffusive tube*

In the two-dimensional pure shear flow, $E_1 = (E_b, 0, -E_b)$, instantaneous pulses elongate exponentially along $x_1$ and diffusively along $x_2$. The continuous source solution should have a similar character such that, unlike the tube, the lengthscale in the $x_2$ direction should grow diffusively as $x_1$ increases. With moments for instantaneous pulses growing exponentially along $x_1$, we expect a logarithmic increase in the $x_2$ lengthscale along $x_1$. The following equation for the concentration $C(\boldsymbol{x})$ results by modifying the assumed concentration distribution of the tube to account for the diffusive growth in the moments in the $x_2$ direction:

$$C(\boldsymbol{x}) = C_c(x_1) \exp\left[\frac{-E_b x_2^2}{2\kappa \ln\left(\frac{E_b x_1^2}{\kappa}\right)} - \frac{E_b x_3^2}{2\kappa}\right], \quad (4.5)$$

where again $C_c$ gives the concentration along the $x_1$ axis. Equating the integral of the concentration distribution over $x_2$ and $x_3$ with the flux from the continuous source as in (4.3) produces the following equation for the centreline concentration of a diffusive tube distribution:

$$C_c(x_1) = C_0 \frac{x_0}{|x_1|} \frac{1}{\left[\ln\left(\frac{E_b x_1^2}{\kappa}\right)\right]^{\frac{1}{2}}}. \quad (4.6)$$

The approximate analytical solution agrees well with the concentration distribution along the diffusive tube centreline (figure 2*a*). In the $x_2$ direction the concentration distribution deviates from that predicted by (4.5) in the region $x_2 > x_1$ (figure 2*b*)), but the deviation is insignificant to the flux analysis since the concentration in this region is several orders of magnitude below the centreline value. By assuming that $x_2 \gg x_1$ and $x_3 = 0$ the convolution integral (3.3) can be integrated directly to give

$$C = C_0 \exp(-x_2/x_0), \quad (4.7)$$

which agrees well with the exact numerical solution in the region where $x_2 > x_1$ (figure 2*b*).

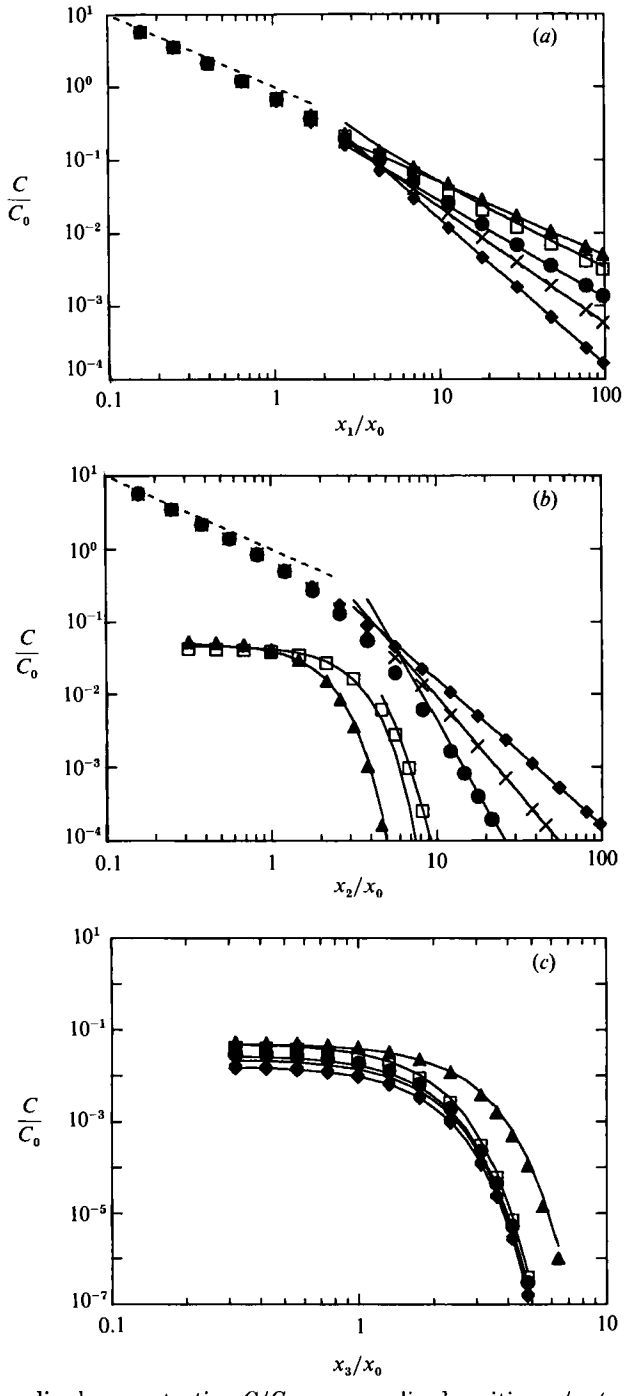


FIGURE 2. Normalized concentration $C/C_0$ *vs.* normalized position $\boldsymbol{x}/x_0$ (see (4.1) for characteristic scales $x_0$ and $C_0$). Symbols give numerical solution of the convolution integral (2.1), while the solid lines give the approximate analytical solutions (§4). The dashed line gives the motionless diffusion analytical solution $C/C_0 = x_0/x_i$. (*a*) Distributions along the line $(x_1/x_0, 0, 0)$ for: $s = 1.0$ (◆), $s = 0.75$ (×), $s = 0.5$ (●), $s = 0$ (□), $s = -1.0$ (▲). (*b*) Distributions along the line $(10, x_2/x_0, 0)$ for: $s = -1.0$ (▲), $s = 0$ (□) (solid line on right gives approximate analytical solution for: $x_2 > x_1$); and along the line $(0, x_2/x_0, 0)$ for: $s = 0.5$ (●), $s = 0.75$ (×), $s = 1.0$ (◆). (*c*) Distributions along the line $(10, 0, x_3/x_0)$ for: $s = -1.0$ (▲), $s = 0$ (□), $s = 0.5$ (●), $s = 0.75$ (×), $s = 1.0$ (◆).

### 4.3. *Disk*

An analogous flux analysis for a disk requires that the flow be axisymmetric in the $(x_1, x_2)$-plane, that is $E_1 = E_2 = -\frac{1}{2}E_3 = \frac{1}{2}E_b$ and $s = 1$. In this case the flux equation can be written as

$$F = \tfrac{1}{2}E_b l \int_{-\infty}^{\infty} C_d(l) \exp\left[\frac{E_3 x_3^2}{2\kappa}\right] dx_3, \tag{4.8}$$

where $C_d$ is the concentration in the axisymmetric $(x_1, x_2)$-plane and $l = (x_1^2 + x_2^2)^{\frac{1}{2}}$ is the distance from the source in the $(x_1\, x_2)$-plane. Integrating across $x_3$ leads to the following equation for thc concentration distribution:

$$C(\boldsymbol{x}) = \left(\frac{8}{\pi}\right)^{\frac{1}{2}} C_0 \left[\frac{x_0}{l}\right]^2 \exp\left[\frac{E_3 x_3^2}{2\kappa}\right]. \tag{4.9}$$

For non-axisymmetric disks ($0 < s < 1$) our flux analysis is indeterminate because we are unable to state *a priori* the shape of concentration contours in the $(x_1, x_2)$-plane. We can, however, find the concentration distribution along either expansive axis by direct integration of (3.3) with $x_1 = 0$ or $x_2 = 0$, which results in the following equation:

$$C(x_1, 0, 0) = \left(\frac{2}{\pi}\right)^{\frac{1}{2}} C_0 \frac{\frac{1}{2}(E_2/E_1)^{\frac{1}{2}} \Gamma(\frac{1}{2}E_b/E_1)}{\left(\dfrac{E_1 x_1^2}{2\kappa}\right)^{\frac{1}{2}E_b/E_1}}. \tag{4.10}$$

Comparison of (4.10) and (4.9) with the previous equations shows that in the sheared region for both tubes and disks the concentration decreases along an expansive axis $i$ as $x_i^{E_i/E_b}$. The concentration distribution along the second expansive axis in a non-axisymmetric disk can be found using (4.10) with a change of indices. The approximate analytical solution (4.10) agrees well with the concentration distributions derived numerically for several axisymmetric and non-axisymmetric disks (figure 2) in the region where advective transport dominates diffusive transport.

While we cannot describe analytically the shape of concentration contours in the expansive plane of non-axisymmetric disks, we can show that the size of a contour is unaffected by changes in the asymmetry of shearing. Assuming advective transport in the expansive $(x_1, x_2)$-plane, the outward flux across a contour $(C = C_z)$ can be written as

$$\text{Flux} = F_{x_1} + F_{x_2} = C_z\left(\frac{2\pi\kappa}{-E_3}\right)^{\frac{1}{2}}\left[\int_{x_2(\min)}^{x_2(\max)} E_1 f^{-1}(x_2)\, dx_2 + \int_{x_1(\min)}^{x_1(\max)} E_2 f(x_1)\, dx_1\right] \tag{4.11}$$

with the integration limits set for a particular concentration contour according to (4.10). The unknown function $f$ and its inverse $f^{-1}$ describe the shape of the contour in the $(x_1, x_2)$-plane such that $C(x_1, f(x_1)), 0 = C_z$. The flux equation (4.11) has already been integrated in the $x_3$ direction using the assumed concentration distribution for axisymmetric disks. Integrating (4.11), noting that $E_b = E_1 + E_2 = -E_3$, results in the following relation for the area of the concentration contour in the $(x_1, x_2)$-plane:

$$\text{Area}\Big|_{\substack{C \geqslant C_z \\ x_3 = 0}} = \frac{F}{(2\pi\kappa E_b)^{\frac{1}{2}} C_z} = (8\pi)^{\frac{1}{2}} \frac{C_0}{C_z} x_0^2. \tag{4.12}$$

For a given intensity of shear $E_b$ and a flux rate $F$, the area bounded by a contour in the $(x_1, x_2)$-plane is independent of the asymmetry of the shearing, though the shape of the contour will be affected by changes in the symmetry factor. The volume

bounded by a contour is also approximately independent of the symmetry factor since the concentration distributions are flattened along the compressive $x_3$ direction and the strength of the shearing in this direction is unaffected by changes in the symmetry factor.

## 5. Continuous point sources in steady rotational shear flows

In this section we describe the shape and orientation of concentration distributions when the shear flow includes rotational components. We examine the deformation of instantaneous pulses using a kinematic model justified by the observation, based on (2.3) that the eigenvectors of the moment tensor for a pulse in any linear flow field are real and orthogonal. Deformation of a pulse can therefore be seen as the superposition of an extensional motion that changes the lengthscales of the pulse together with an angular motion that reorients the pulse. Pulses in rotational flows are turned from the principal axes of strain so that the extensional motion varies in time. When the rotation is weak relative to the shearing, instantaneous pulses rotate to an equilibrium orientation where the angular motion is zero (Lumley 1972). Extension rates along the equilibrium orientation axes are equal to a weighted average of the extension rates along the principal axes of strain. For strongly rotational flows the concentration distribution is the same as that resulting from an axisymmetric, irrotational flow with an axis of symmtry along the rotation axis (Batchelor 1979). The extension rate along the axis of symmetry for the equivalent irrotational flow is the component of the rate of strain tensor in the direction of the rotation vector for the strongly rotational flow.

To analyse the effects of rotation we examine how changing the strength of the rotation component changes the dimensions of a concentration contour when viewed from the equilibrium orientation. Concentration distributions are calculated using the convolution integral for a series of velocity gradient tensors, each with an identical shear component, and with rotation components that vary in intensity but not in orientation. This analysis is done initially with a simple specification of rotation, where the rotation axis is aligned with a principal axis of strain. The criterion for weak rotation, which requires that an equilibrium orientation exists, is analysed for this simple rotational case and later for a general velocity gradient tensor. We then look at a more general rotational shearing flow where the rotation axis is not aligned with a principal axis of strain. In both examples we show that the critical rotation rate is the key parameter which determines the effect of rotation on the shape of the concentration distributions.

### 5.1. *Concentration distributions with rotation along a principal axis of strain*

With the rotation axis aligned along a principal axis of strain it is possible to derive simple equations describing the angular location of the equilibrium orientation relative to the principal axes of strain and the extension rates along the equilibrium orientation. The rotational shearing flow analysed has a fixed shear component ($s = -0.6$) and a vorticity component of varying intensity $\omega$ that is aligned with $x_2$ such that $\boldsymbol{\omega} = (0, \omega, 0)$. The equilibrium orientation can be found for this special case by determining the directions in which the angular component of the motion is zero. The equilibrium orientation turns from the principal axes around the $x_2$ axis by an angle $\alpha$, such that

$$\alpha = \tfrac{1}{2}\sin^{-1}\left(\frac{\omega}{E_1 - E_3}\right). \tag{5.1}$$

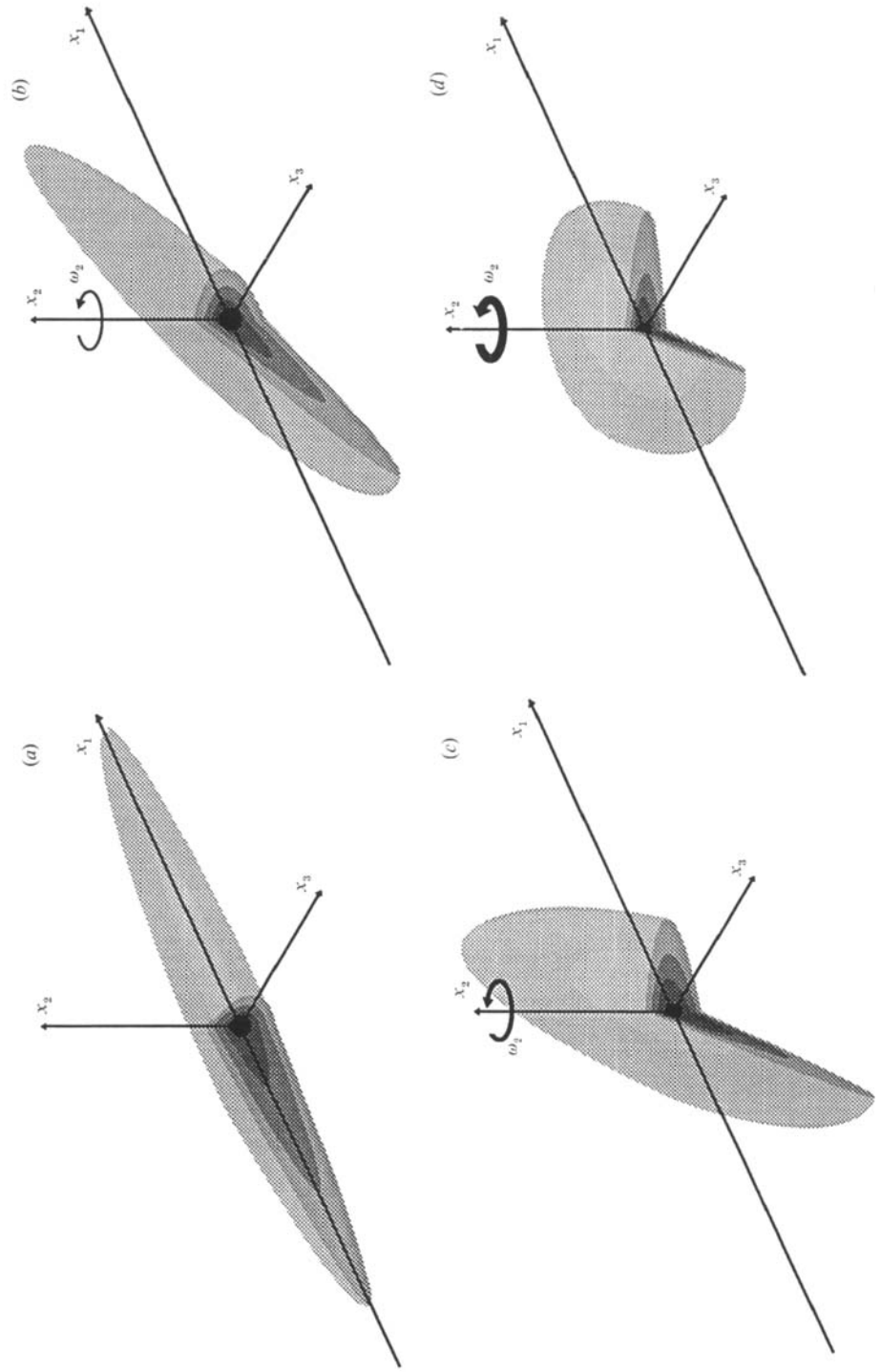


FIGURE 3. Qualitative features of the concentration distributions in a shear flow with principal strain rates $(E_b, -0.3E_b, -0.7E_b)$ and a vorticity vector $(0, \omega_2, 0)$ of increasing intensity $\omega_2$: (*a*) no rotation, $\omega_2/\omega_{crit} = 0$, tube lies along the $x_1$ axis; (*b*) $\omega_2/\omega_{crit} = 0.9$, tube is rotated 30° from the $x_1$ axis; (*c*) $\omega_2/\omega_{crit} = 2.0$, tube is now stretched laterally and rotated 45°; (*d*) $\omega_2/\omega_{crit} = 10.0$, distribution is now a disk, approaching axisymmetry about the $x_2$ axis. Characteristic dimensions of the distribution as a function of rotational strength are shown quantitatively in figure 4.

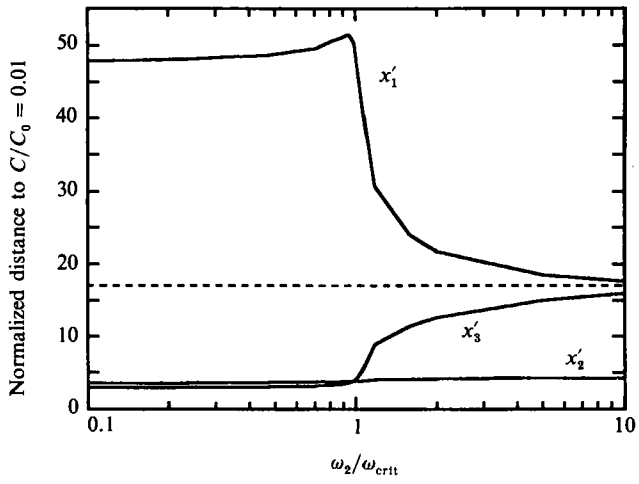


FIGURE 4. Normalized distances ($x_i'/x_0$) from the source to the concentration level $C/C_0 = 0.01$ along each rotated coordinate axis *vs.* the normalized vorticity $\omega_2/\omega_{crit}$ for the vorticity vector $(0, \omega_2, 0)$ and principal strain rates $(E_b, -0.3E_b, -0.7E_b)$. The horizontal dashed line represents the normalized distance to $C/C_0 = 0.01$ along expansive axes for the strong rotation limit that is equivalent to an axisymmetric shearing with principal strain rates $(0.3E_b, -0.6E_b, 0.3E_b)$.

The vorticity can be normalized to the critical value for the existence of an equilibrium orientation ($\omega_{crit} = E_1 - E_3$) as

$$\omega_* = \frac{\omega_2}{\omega_{crit}} = \frac{\omega}{E_b(2 - \frac{1}{2}|s|)}. \tag{5.2}$$

For weak rotation ($\omega_* < 1$), the extension rates along the two rotated axes of the equilibrium orientation, $x_1'$ and $x_3'$, can be specified as

$$E_1'/E_b = -\tfrac{1}{4}s + (1 - \tfrac{1}{4}|s|)(1 - \omega_*^2)^{\frac{1}{2}}, \tag{5.3}$$

$$E_3'/E_b = -\tfrac{1}{4}s - (1 - \tfrac{1}{4}|s|)(1 - \omega_*^2)^{\frac{1}{2}}. \tag{5.4}$$

The extension rate along $x_2'$ ($E_2'$) is unaffected by vorticity since the rotation axis is aligned with $x_2$ (Batchelor 1979).

The distance to a constant concentration level ($C/C_0 = 0.01$) in the sheared region was calculated along each equilibrium orientation axis for both weak and strong rotation. The irrotational shear component ($s = -0.6$) produces a concentration distribution that is a non-axisymmetric tube with a centreline aligned with $x_1$ (figure 3). For strong rotation cases ($\omega_* > 1$) the distance to $C/C_0 = 0.01$ was calculated at $\alpha = 45°$. Normalized concentrations and distances (see (4.1)) were calculated using the irrotational shear component. The concentration distribution for the strong rotation limit is an axisymmetric disk ($s = 1.0$) with an axis of symmetry along $x_2$ (figure 3). The characteristic shear rate for the strong rotation limit ($E_b'$) is less than the characteristic shear rate for the irrotational shear case ($E_b'/E_b = 0.3$).

The effect of the rotation on the distributions is small for most of the weak rotation region ($\omega_* < 1$) see (figures 3 and 4). For normalized rotation rates below approximately 0.95, the dimensions of the concentration contour change little from the irrotational pattern (figure 4). The orientation of the concentration distribution does change significantly, however, since the equilibrium orientation axes $x_1'$ and $x_3'$ rotate around $x_2$ by 33.2° at $\omega_* = 0.9$. As the vorticity intensity is increased past the critical value, the dimensions of the concentration contour change quickly and by

$\omega_* = 2.0$ the long axis of the contour is only twice the length of the other axis in the plane perpendicular to the rotation vector. At higher rotation rates the distribution approaches the limiting axisymmetric distribution with the axis of symmetry along the rotation axis (figure 4).

In this example the effect of rotation is to turn a tube-like distribution (figure 3*a*) into a disk-like one (figure 3*d*). The critical rotation rate for the existence of an equilibrium orientation is shown to be the key parameter in describing the shape of the distributions. In the next section we derive the criterion for this critical rotation rate for a general velocity gradient tensor.

### 5.2. *A general conditions for the critical rotation rate*

No simple geometrically based relationship for the critical rotation rate is possible for a general vorticity vector. Nonetheless we can use information on the velocity gradient tensor to determine the critical rotation rate for any general linear flow described by (1.3). An equilibrium orientation must be described by a set of real vectors, which in turn requires that the extension rates along the equilibrium orientation be real, since our solution must have no imaginary part. Since the equilibrium orientation and the eigenvectors of the velocity gradient tensor form right and left eigenvector pairs (Lumley 1972), then all three eigenvalues of the velocity gradient tensor must also be real when an equilibrium orientation exists.

A characteristic polynomial giving the eigenvalues of $\boldsymbol{G}$ is $y^3+ay+b=0$, where $a=\frac{1}{4}(\omega_i\omega_i)-\frac{1}{2}(E_iE_i)$, and $b=-(E_1E_2E_3+\frac{1}{4}E_i\omega_i\omega_i)$. The coordinate system used is formed by the principal axes of strain. The roots of the polynomial are the eigenvalues of the velocity gradient tensor $\boldsymbol{G}$. The condition that all the roots of the polynomial are real can be used to provide the following condition for weak rotation:

$$E_iE_i-\tfrac{1}{2}(\omega_i\omega_i) > 3\times 2^{\frac{1}{3}}(E_1E_2E_3+\tfrac{1}{4}E_i\omega_i\omega_i)^{\frac{2}{3}}. \tag{5.5}$$

For a given irrotational shear component and direction for the vorticity vector, a normalized rotation rate can be defined as $\omega_* = (\omega_i\omega_i)^{\frac{1}{2}}/\omega_c$, where $\omega_c$ is the magnitude of the vorticity vector that makes (5.5) an equality. When the rotation is weak ($\omega_* < 1$), an instantaneous pulse will rotate to a stable orientation and subsequent deformation of the pulse will be determined by the components of the rate of strain tensor in the equilibrium orientation. At rotation rates above the critical value ($\omega_* > 1$), the velocity gradient tensor will have one real eigenvalue with two imaginary eigenvalues that are complex conjugates, giving an oscillatory behaviour to the solution for an instantaneous pulse. The orientation of the pulse will oscillate around an orientation specified by the eigenvectors corresponding to the real part of the velocity gradient's eigenvalues at a frequency equal to the rotation rate. At high rotation rates ($\omega_* \gg 1$) the behaviour of the pulse will be independent of the rotation rate and the pulse will deform in an axisymmetrical fashion with an axis of symmetry aligned with the vorticity vector.

### 5.3. *Concentration distributions for an arbitrary rotation vector*

We can now analyse rotational effects on continuous sources for any combination of shear and rotation components. As in the earlier example we examine the changes in the shape of a concentration contour ($C/C_0 = 0.01$) as the rotation intensity is increased. The shear component is fixed ($s=-0.6$) with a vorticity vector of constant direction $(0,\omega,\omega)$, and a variable intensity $\omega$. Vorticity is normalized to the critical vorticity value which is calculated using (5.5) for $s=-0.6$ so that $\omega_{\text{crit}} = 0.73E_{\text{b}}$. The irrotational limit is the same as in the earlier case, producing a

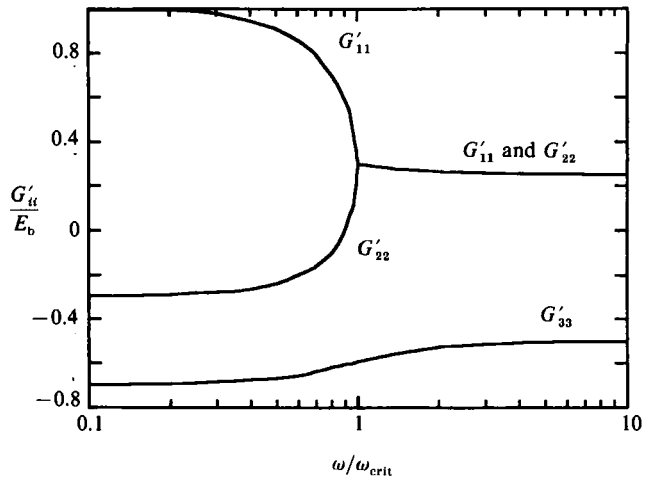


FIGURE 5. Extension rates along each rotated coordinate axis $G'_{ii}$ normalized by the irrotational strain intensity $E_b$ *vs.* the normalized vorticity $\omega/\omega_{crit}$ for the vorticity vector $(0, \omega, \omega)$ with principal strain rates $(E_b, -0.3E_b, -0.7E_b)$.

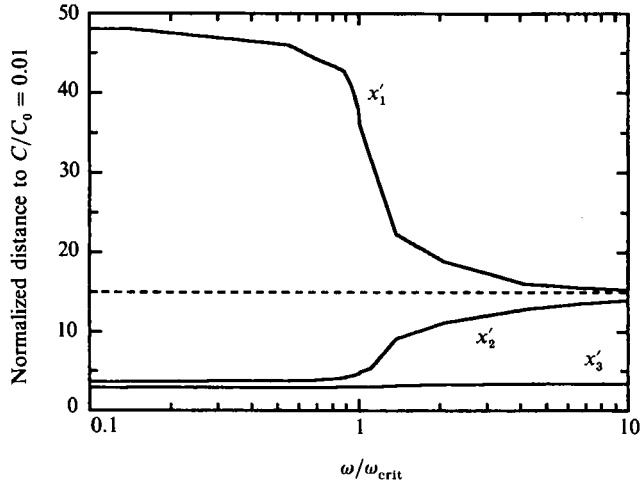


FIGURE 6. Normalized distances $(x'_i/C_0)$ from the source to the concentration level $C/C_0 = 0.01$ along each rotated coordinate axis *vs.* the normalized vorticity $\omega/\omega_{crit}$ for the vorticity vector $(0, \omega, \omega)$ and principal strain rates $(E_b, -0.3E_b, -0.7E_b)$. The horizontal dashed line represents the normalized distance to $C/C_0 = 0.01$ along expansive axes for the strong rotation limit that is equivalent to an axisymmetric shearing with principal strain rates $(0.5E_b, 0.5E_b, -E_b)$.

tube-like distribution for irrotational strain. The concentration distribution expected in the limit of strong rotation is again an axisymmetric disk ($s = 1.0$), but with $E'_b/E_b = 0.5$ rather than 0.3.

As in the previous case, the asymmetry in the shearing rates (figure 5) and in the concentration distributions (figure 6) remains nearly unchanged until the vorticity intensity approaches the critical value. An analysis of the velocity gradient tensor in the coordinate system formed by the equilibrium orientation showed the tensor to have a special form that was used to calculate the extension rates (figure 5). (The analysis is in an Appendix available from the authors or the editor.) Increases in vorticity beyond the critical value change dramatically the shape of the distribution

and the ratio of lengthscales is reduced to below 2.0 by the time the vorticity is twice the critical value. Further increases in vorticity produce concentration distributions approaching the limiting strong rotation case. The limiting lengthscale in this case is slightly larger than in the first case because the strength of the axisymmetric shearing is stronger ($E'_b/E_b = 0.5$ *vs.* 0.3).

## 6. Continuous sources in homogeneous turbulence

In turbulent flows the assumption that the velocity gradient tensor is homogeneous is approximately satisfied if the region of interest is smaller than the Kolmogorov microscale $(\nu^3/\epsilon)^{\frac{1}{4}}$. Since the shear rate $E_b$ is of order $(\epsilon/\nu)^{\frac{1}{2}}$, this constraint may be expressed as $r/x_0 < (\nu/\kappa)^{\frac{1}{2}}$. The Schmidt number $(\nu/\kappa)$ is of order 1000 for small-molecular-weight compounds dissolved in water, which limits the range of interest to dimensionless distances of approximately 30. For typical organic compounds with larger molecular weights (1500 g/mole) the region of interest may be as much as three times larger.

Our steady-state analysis is appropriate if the timescale of variation in the shear rate is long relative to the Kolmogorov timescale. Lumley (1972) has hypothesized that the shearing lasts for a time equal to the Lagrangian integral timescale. The ratio of the Lagrangian integral timescale to the Kolmogorov timescale has been estimated to be of order $R_\lambda^{\frac{1}{2}}$ (Corrsin 1963), where $R_\lambda$ is the Reynolds number calculated using the Taylor microscale $\lambda$. There is, however, some doubt about this hypothesis (Monin & Yaglom 1975), though recent particle tracking experiments show Lagrangian integral timescales in excess of Kolmogorov timescales (Sato & Yamamoto 1987). Unfortunately the Reynolds numbers of these experiments are not high enough to be a true test. The assumption of steady, homogeneous shear is essentially that used by Batchelor (1959) in analysing small-scale variations in scalar quantities.

Recent numerical simulations of homogeneous turbulence examining correlations between shear and vorticity (Kerr 1985) and alignment between component of shear and vorticity (Ashurst *et al.* 1987) can be used in conjunction with our analysis to give a qualitative description of the shape of continuous point source concentration distributions in isotropic turbulence. Ashurst *et al.* (1987) examined the velocity gradient tensor at 16384 uniformly distributed points in space for isotropic turbulence with $R_\lambda = 82.9$. To characterize the strain component they define a normalized principal strain rate nearly equivalent to our symmetry factor $s$ (see (3.4)) as $\beta = E_2\sqrt{6}/(E_t E_t)^{\frac{1}{2}} \approx s$.

In locations with viscous dissipation below the median rate they found that positive and negative values for $\beta$ are equally likely and 75% of the $\beta$ values are between $\beta = 0.5$ and $\beta = -0.5$. When there are two positive principal strain rates ($\beta > 0$) the flow is strongly rotational (average $\omega/\omega_{crit} = 7$). The majority of these locations ($\approx 20\%$ of total) have a vorticity vector aligned with the axis of the intermediate principal strain rate ($E_2$), resulting in tube-like concentration distributions for point sources axisymmetric about the vorticity vector. Extension rates along the vorticity vector are significantly below the average shear rate because of the relatively weak dissipation and the particular alignment of the vorticity vector. In locations with two compressive axes ($\beta < 0$) the rotation is not aligned with either compressive axis, thus these locations also have tube-like concentration distributions.

Ashurst *et al.* report that locations with viscous dissipation above the median value

have two positive principal axes ($\beta > 0$). These high-dissipation regions have an average vorticity level near the average for the entire fluid, thus we expect some concentration distributions shaped as non-axisymmetric disks in weakly rotating locations ($\beta > 0$, $\omega < \omega_{crit}$). However, Kerr (1985) discovered regions of high vorticity in vortex tubes associated with regions of strong shear and with the single compressive strain axis perpendicular to the vortex tube axis. Neither Kerr nor Ashurst *et al.* give the relative magnitude of the shear and vorticity components in the vortex tubes so we cannot determine whether the flow is strongly or weakly rotational. With the observed alignment of strain and vortical components, however, a strongly rotational vortex tube results in tube-like concentration distributions aligned with the vorticity vector while weakly rotational flow results in disk-like concentration distributions.

Summarizing the results for the entire turbulent fluid, we expect that tube-like concentration distributions are more common than disks even though regions with $\beta > 0$ occupy a majority of the fluid (Ashurst *et al.* report 75%). The preponderance of locations with two positive principal strain rates is consistent with a similar analysis by Townsend (1951*b*). Of interest, however, is the relative strength of the vorticity and its alignment with a positive principal strain rate, which results in axisymmetric tube-like concentration distributions for strong rotation even though the irrotational shear alone would result in disk-like distributions. Strongly rotational axisymmetric tubes occupy at least half of the locations with viscous dissipation below the median rate ($\approx 20\%$ of total volume) and are also expected in strongly rotational vortex tubes with strain rates significantly above the median level. Disk-like concentration distributions are found only in locations where viscous dissipation is above the median value and the rotation is weak relative to the shear ($< 50\%$ of total volume). Flatness factors for shear and vorticity are significantly above uncorrelated levels (Kerr 1985), so that median levels of fluid motion, and consequently the distortion of concentration distributions by fluid motion, are below estimates based on average conditions.

This research was supported by the National Science Foundation under Grants OCE-8614488 and CES-8801767. J.D.B. acknowledges the support of a Hugh Hampton Young Fellowship. The authors would like to thank S. W. Chisholm, J. B. Waterbury, and P. M. Gschwend for their assistance and comments.

## REFERENCES

Ashurst, W. T., Kerstein, A. R., Kerr, R. M. & Gibson, C. H. 1987 Alignment of vorticity and scalar gradient with strain rate in simulated Navier–Stokes turbulence. *Phys. Fluids* **30**, 2343.

Batchelor, G. K. 1959 Small-scale variation of convected quantities like temperature in turbulent fluid. Part 1. General discussion and the case of small conductivity. *J. Fluid Mech.* **5**, 113.

Batchelor, G. K. 1979 Mass transfer from a particle suspended in fluid with a steady linear ambient velocity distribution. *J. Fluid Mech.* **95**, 369.

Carslaw, H. S. & Jaeger, J. C. 1959 *Conduction of Heat in Solids*. Oxford University Press.

Corrsin, S. 1963 Estimates of the relation between Eulerian and Lagrangian scale in large Reynolds number turbulence. *J. Atmos. Sci.* **20**, 115.

Csanady, G. T. 1973 *Turbulent Diffusion in the Environment*. D. Reidel.

Elrick, R. E. 1962 Source functions for diffusion in uniform shear flow. *Austral. J. Phys.* **15**, 283.

Foister, R. T. & Van den Ven, T. G. M. 1980 Diffusion of brownian particles in shear flows. *J. Fluid Mech.* **96**, 105.

KERR, R. M. 1985 Higher-order derivative correlations and the alignment of small-scale structures in isotropic numerical turbulence. *J. Fluid Mech.* **153**, 31.

LUMLEY, J. L. 1972 On the solution of equations describing small scale deformation. In *Symposia Matematica: Convegno sulla Teoria delta Turbolenza al Istituto Nazionale di Alta Matematica*, pp. 315–334. Academic.

MONIN, A. S. & YAGLOM, A. M. 1975 *Statistical Fluid Mechanics*, vol. 2. MIT Press.

NOVIKOV, E. A. 1958 Concerning turbulent diffusion in a stream with a transverse gradient of velocity. *Prikl. Math. Mech.* **22**, 412.

OKUBO, A. & KARWEIT, M. J. 1969 Diffusion from a continuous source in a uniform shear flow. *Limnol. Oceanogr.* **14**, 514.

SATO, Y. & YAMAMOTO, K. 1987 Lagrangian measurement of fluid-particle motion in an isotropic turbulent field. *J. Fluid Mech.* **175**, 183.

SMITH, R. 1981 The early stages of contaminant dispersion in shear flows. *J. Fluid Mech.* **111**, 107.

SMITH, R. 1982 Dispersion of tracers in the deep ocean. *J. Fluid Mech.* **123**, 131.

TENNEKES, H. & LUMLEY, J. L. 1972 *A First Course in Turbulence.* MIT Press.

TOWNSEND, A. A. 1951*a* On the fine-scale structure of turbulence. *Proc. R. Soc. Lond.* **A208**, 534.

TOWNSEND, A. A. 1951*b* The diffusion of heat spots in isotropic turbulence. *Proc. R. Soc. Lond.* **A209**, 418.

TURFUS, C. 1986 Diffusion from a continuous source near a surface in steady reversing shear flow. *J. Fluid Mech.* **172**, 183.